Simulation of Fractal Multidimensional Images Using Multidimensional Recursive Filters

L. T. Bruton and N. R. Bartley

Abstract—**Fractal multidimensional (MD) images may be generated by simulating MD fractal Brownian motion (fBm). This is usually achieved by appropriately weighting the magnitudes of the Fourier coefficients of the MD discrete Fourier transform (DFT) of the required fractal image. In this contribution, it is proposed that MD hyperspherically-symmetric recursive filters be used to approximate fractal images directly in the spatial domain, thereby allowing spatially-variant characteristics to be obtained without the undesirable edge effects of the MD DFT method. The method is used to generate realistic 2D fractal landscape images having spatially-variant characteristics.**

I. Introduction

MANDELBROT'S FRACTAL GEOMETRY [1] has found a wide variety of applications. The statistical self-similarity of fractal shapes is inherent in the natural world and may be exploited to simulate natural processes. In [2], Voss describes the self-similarity of fractal landscapes and distinguishes between deterministic fractals, such as the von Koch snowflakes, and random fractals. In particular, random fractional Brownian motion (fBm) corresponds to fractal landscapes and occurs widely in nature, accurately describing such phenomena as pitch variation in music, flicker noise in solid-state devices, 2D mountain landscapes and 3D spatio-temporal image sequences of moving formations of clouds [2].

The analysis and synthesis of 1D fBm has been of growing interest recently, and recent publications have appeared [3], [4] that explore fBm using wavelet-based techniques. In this contribution, it is shown that multidimensional (MD) fBm may be simulated in the spatial domain by applying MD noise, having a known MD spectral density function, to a MD hyperspherically-symmetric recursive digital filter.

Following [2], a MD continuous-domain signal $x(\mathbf{t})$, $\mathbf{t} \in R^M$, possesses fBm if, throughout its domain, the MD difference $\Delta(\mathbf{t}_1, \mathbf{t}_2) \equiv x(\mathbf{t}_1) - x(\mathbf{t}_2)$ satisfies the following stochastic properties; for any $\mathbf{t}_1$ and $\mathbf{t}_2, \mathbf{t}_1 \neq \mathbf{t}_2$, in the domain of $x(\mathbf{t})$,

1) $\Delta(\mathbf{t}_1, \mathbf{t}_2)$ is a zero-mean function having a Gaussian amplitude probability density function and,
2) the variance $\sigma(\mathbf{t}_1, \mathbf{t}_2)$ of $\Delta(\mathbf{t}_1, \mathbf{t}_2)$ is given, for some constant K, by

$$\sigma(\mathbf{t}_1, \mathbf{t}_2) = K[||\Delta(\mathbf{t}_1, \mathbf{t}_2)||_2]^H, H,\ K,\ \in R \tag{1}$$

where $||\Delta(\mathbf{t}_1, \mathbf{t}_2)||_2$ is the MD Euclidean norm. The scaling parameter H controls the relative "roughness" (or "smoothness") of the continuous-domain MD fractal surface $x(\mathbf{t})$.

The concept of *fractal dimension* D is often used [2] to characterize fractal surfaces, where

$$D \equiv M + 1 - H \tag{2}$$

and where M is the dimensionality of $x(\mathbf{t})$. Generally, the fractal dimension D is in the range $M \leq D \leq M + 1$, corresponding to $0 \leq H \leq 1.0$. For example, in the 2D case ($M \equiv 2$), it has been found that $H \approx 0.8$ corresponds to excellent 2D surface simulations of mountainous landscapes. The fractal dimension of the landscape is then given by $D = 2 + 1 - 0.8 = 2.2$.

Let $X(j\boldsymbol{\omega})$, $\boldsymbol{\omega} \in R^M$, be the MD Fourier transform of $x(\mathbf{t})$ so that $\Phi(\boldsymbol{\omega}) \equiv X(j\boldsymbol{\omega})X(-j\boldsymbol{\omega}) = |X(j\boldsymbol{\omega})|^2$ is the real continuous-domain MD spectral density function of $x(\mathbf{t})$. It is well known that [2], [6] this MD fBm has the spectral density function

$$\Phi(\omega) = \frac{\Phi_0}{[||\boldsymbol{\omega}||_2]^{2H+1}}, \Phi_0 \text{ constant } \in R \qquad \text{SPECTRAL DENSITY FUNCTION OF MD fBm} \tag{3}$$

where $||\boldsymbol{\omega}||_2$ is the Euclidean norm of the MD vector $\boldsymbol{\omega}$; that is, $||\boldsymbol{\omega}||_2$ is the Pythagorean distance of $\boldsymbol{\omega}$ from the origin in R^M. The parameter β, where

$$\beta \equiv 2H + 1 \tag{4}$$

is referred to as the *spectral exponent* of the fBm, so that

$$\Phi(\boldsymbol{\omega}) = \Phi_0||\boldsymbol{\omega}||_2^{-\beta}, \Phi_0, \beta \in R. \tag{5}$$

Typically, for the case of a 2D landscape, one might choose $H = 0.8$, implying $\Phi(\boldsymbol{\omega}) = \Phi_0[||\boldsymbol{\omega}||_2]^{-2.6}$ and $|X(\boldsymbol{\omega})| = \Phi_0^{1/2} [||\boldsymbol{\omega}||_2]^{-1.3}$.

Manuscript received June 4, 1991; revised September 22, 1993. This work was supported in part by Micronet, the Federal Centre of Excellence on Microelectronic Devices, Circuits and Systems, and the Natural Sciences and Engineering Research Council of Canada. This paper was recommended by Associate Editor K. H. Tzou.

The authors are with the Department of Electrical and Computer Engineering, University of Calgary, Calgary, Alberta, Canada.

IEEE Log Number 16360.

1057-7130/94$04.00 © 1994 IEEE

II. Review of the Simulation of MD fBm Using Direct Spectral Synthesis and the Discrete Fourier Transform

We are concerned with a *discrete-domain* sampled version of $x(\mathbf{t})$, which we write as $x(\mathbf{n})$, $\mathbf{n} \in Z^M$, where the values of $x(\mathbf{n})$ are quantized in machine-representable form. Clearly, $x(\mathbf{n})$ can only be a discrete-domain quantized-amplitude *approximation* of a continuous-domain signal $x(\mathbf{t})$; this follows because the statistical distributions of $\Delta(\mathbf{n}_1, \mathbf{n}_2) \equiv x(\mathbf{n}_1) - x(\mathbf{n}_2)$ are *not defined* for non-integer values of $\mathbf{n}_1$ and $\mathbf{n}_2$ and one cannot consider a corresponding image surface to have any meaning at spatial resolutions near or below one sample distance. However, at much larger MD spatial distances where $||\mathbf{n}_1 - \mathbf{n}_2||_2 \gg 1$, the continuous surface (obtained by connecting rectangularly adjacent samples of $x(\mathbf{n})$ with planar surfaces) turns out to provide an excellent approximation to the continuous-domain fBm function $x(\mathbf{t})$. This is achieved by ensuring that the *discrete-domain* spectral density function $\Phi(\mathbf{\Omega})$, $\mathbf{\Omega} \in Z^M$, approximates (3) over an appropriate region of support. The DFT has been widely used for this purpose [2], [6]. We write the DFT of $x(\mathbf{n})$ as $X(\mathbf{\Omega})$ and assume MD regions of support for $x(\mathbf{n})$ and $X(\mathbf{\Omega})$ given by

$$Z^M \equiv \{\mathbf{n} | -M_i/2 \leq n_i \leq (M_i - 1)/2, \forall n_i, i = 1..M\} \quad (6)$$

A. Direct Spectral Synthesis

Discrete-domain MD fBm signals are obtained by choosing the discrete-domain MD complex coefficients $X(\mathbf{\Omega})$, such that

$$E[|X(\mathbf{\Omega})|] = \frac{B}{[||\mathbf{\Omega}||_2]^\beta}, \forall \Omega \in Z^M \quad (7)$$

where E denotes expected value, and such that $argX(\mathbf{\Omega})$ is randomly chosen with uniform probability in the interval $[0\ 2\pi]$ [6]. The inherent conjugate symmetries of $X(\Omega)$ in Z^M require that $|X(\mathbf{\Omega})|$ be computed over only $1/2^M$ of the discrete points in Z^M. At the M-tuple $\mathbf{\Omega} \equiv \{\Omega_1, \Omega_2, \ldots, \Omega_M\}$, the magnitude of the corresponding coefficient $|X(\mathbf{\Omega})|$ is given by [6]

$$|X(\mathbf{\Omega})| = \frac{|\text{Gauss}|}{[||\mathbf{\Omega}||_2]^\beta} \quad (8)$$

where *Gauss* is a procedure call that generates real numbers (each time the procedure is called) having zero mean and unity variance. For the 2D case, the corresponding inverse 2D DFT, $x(n_1, n_2) = \text{DFT}^{-1}[X(\mathbf{\Omega})]$, has been shown to approximate excellent natural-looking surface landscapes and is the basis for the computer-based simulation of fractal-based scenes.

The above *direct spectral synthesis* method does have certain practical limitations. Obviously, to achieve the required spectral distribution, it is necessary to choose a sufficiently large region of support Z^M; typically, the image size M_i in the ith dimension must exceed 512 sample points, for all dimensions $i = 1, 2, \ldots, M$. In the 2D case, this corresponds to $512^2 = 262,144$ data points per block of $x(n_1, n_2)$ and a 2D fractal surface that can, at most, possess self-similarity over a magnification (zoom) factor of about 100, at which point the resolution is so coarse that 'surface' features are not visually interpreted by the human vision system.

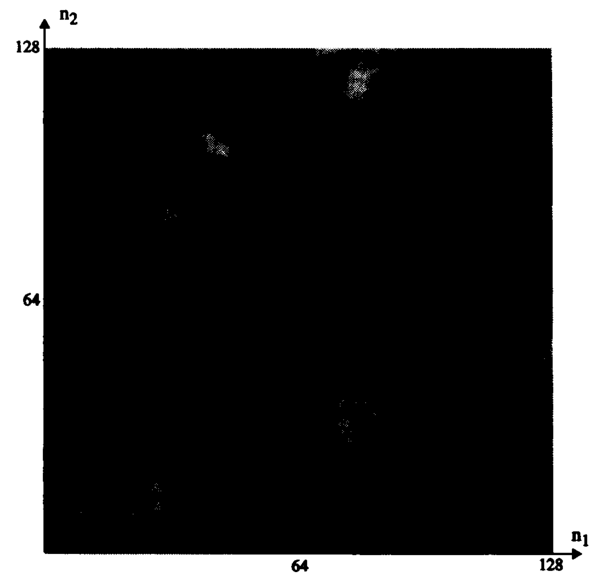

Fig. 1. Fractal image produced by the 2D DFT method using four blocks, $M_1 = M_2 = 64$.

The DFT synthesis method has additional limitations. The number of real multiplications $N^{(\text{FFT})}_{\text{mult}}$ and real additions $N^{(\text{FFT})}_{\text{add}}$, assuming a fast Fourier transform (FFT) implementation of the DFT is given, for the 2D case, by

$$\begin{aligned} N^{(\text{FFT})}_{\text{add}} &= 3M_1M_2\log_2(M_1M_2) \\ N^{(\text{FFT})}_{\text{mult}} &= 2M_1M_2\log_2(M_1M_2). \end{aligned} \quad (9)$$

This often imposes a practical limit on the maximum block size that can be processed by the FFT in an acceptable period of time. The coverage of very large images $x(\mathbf{n})$, say $M_i > 10^4$, is often only practical if $x(\mathbf{n})$ is broken into smaller rectangles and by applying the FFT to each rectangular block. However, block processing causes intolerable edge effects, as shown in Fig. 1 for the 2D case, where $M_1 = 64$ and $M_2 = 64$ in each of the four rectangular blocks.

A final disadvantage of the DFT approach is that it is not possible to spatially-vary the statistics of the fractal image within each data block. The spectral exponent β, and therefore the overall appearance of the surface features, are necessarily constant (independent of $\mathbf{n}$) in each block of Fig. 1. It would be very useful, from a practical point of view, if the "roughness" of the fractal surface could be arbitrarily varied throughout the image $x(\mathbf{n})$ by choosing $\beta(\mathbf{n})$ to be a function of $\mathbf{n}$. In this way, mountains could merge gradually into smooth valleys, for example, without the requirement for postprocessing of the fractal image [2]. It might also be desirable to spatially-vary the exponent β as a function of angular orientation so that surfaces are "rougher" in some directions than in other directions, thereby attributing *direction-oriented texture and roughness* to a surface.

III. Approximation of MD fBm Using Recursive MD Filters Excited by MD Noise

Assume a continuous-domain MD noise source $x(\mathbf{t})$ having a Gaussian amplitude probability function, zero mean and unity variance. Let the MD Fourier transform of $x(\mathbf{t})$ be $X(j\boldsymbol{\omega})$ and assume that the corresponding MD spectral density function $\Phi_x(\boldsymbol{\omega})$ is known and note that $\boldsymbol{\omega} \in R$.

In practice, we require a discrete-domain version $x(\mathbf{n})$ of this noise process having region of support Z^M, for which the corresponding continuous-domain spectral density function $\Phi_x(\boldsymbol{\omega}) = X(j\boldsymbol{\omega})X(-j\boldsymbol{\omega})$ is also defined on R^M, but has periodicity 2π in each frequency variable ω_i. We define the hyperrectangular region R_π^M of R^M as

$$R_\omega^M \equiv \{\boldsymbol{\omega} \in R^M| - \pi \leq \omega_1, \omega_2, \ldots, \omega_M \leq \pi\} \tag{10}$$

and we propose to approximate the spectral density function $\Phi(\omega)$ of (3) over this region. Consider a prototype discrete-domain MD noise signal $x(\mathbf{n})$ ideally having the continuous-domain MD spectral density function $\Phi_x(\boldsymbol{\omega}) = \Phi_{x0}(||\boldsymbol{\omega}||_2)^{-\alpha}$, $\boldsymbol{\omega} \in R_\pi^M$. Let $x(\mathbf{n})$ be applied to a MD digital filter having a unit impulse response $h(\mathbf{n})$ and a MD hyperspherically-symmetric continuous-domain energy density spectrum $\Phi_h(\boldsymbol{\Omega})$ given by

$$\Phi_h(\boldsymbol{\omega}) \equiv H(j\boldsymbol{\omega})H(-j\boldsymbol{\omega}) = \Phi_{h0}[||\boldsymbol{\omega}||_2]^{-\beta_h}, \boldsymbol{\omega} \in R_\pi^M \tag{11}$$

where $H(j\boldsymbol{\omega})$ is the Fourier transform $F[h(\mathbf{n})]$ and the magnitude response $M(\boldsymbol{\omega})$ is given by

$$M(\boldsymbol{\omega}) \equiv |H(j\boldsymbol{\omega})| = \Phi_{h0}^{1/2}[||\boldsymbol{\omega}||_2]^{-\beta_h/2}, \quad \boldsymbol{\omega} \in R_\pi^M. \tag{12}$$

Writing

$$\beta \equiv \alpha + \beta_h, \tag{13}$$

it follows that the MD output signal $y(\mathbf{n}) = (x(\mathbf{n}) * h(\mathbf{n}))$ has a corresponding continuous-domain spectral density function $\Phi_y(\boldsymbol{\omega})$ given by

$$\Phi_y(\boldsymbol{\omega}) = \Phi_x(\boldsymbol{\omega})\Phi_h(\boldsymbol{\omega}) = \Phi_{y0}[||\boldsymbol{\omega}||_2]^{-\beta}, \boldsymbol{\omega} \in R_\pi^M \tag{14}$$

where Φ_{y0} is defined as $\Phi_{x0}\Phi_{h0}$. Equation (14) corresponds to one MD period of $\Phi_y(\omega)$ in R^M and is the required spectral density function of the discrete-domain simulated fBm signal $y(\mathbf{n})$.

It is interesting to note that MD recursive filters are well suited to simulate MD fBm in this way. In general, $1/f$-type noise is characterized as having long-range dependency, or "memory", where current values of a process are influenced by its entire history, most strongly by recent events and by decaying amounts for increasingly distant events [5]. We employ MD recursive filters to model this notion of memory via the convolution operation $y(\mathbf{n}) = x(\mathbf{n}) * h(\mathbf{n})$. It is important to recognize that the impulse responses $h(\mathbf{n})$ of these filters are *exponential* in nature and can only approximate the *power-law* decay of the fBm.

In the remainder of this contribution, we describe a 2D application of this principle using 'white' 2D noise ($\alpha \equiv 0$) as the input signal $x(n_1, n_2)$ to a 2D recursive digital filter $h(n_1, n_2)$ that is designed to have an approximately circularly-symmetric magnitude frequency response function $M(\omega_1, \omega_2)$.

IV. Generation of 2D Fractal Landscape Approximations Using Recursive Digital Filters

Choosing the spectral exponent α of the 2D noise samples $x(n_1, n_2)$ as zero corresponds to an easily-implemented spectrally-flat noise source. We must then implement a 2D recursive filter such that its *continuous-domain circularly-symmetric* magnitude frequency response is given by

$$M(\omega_1, \omega_2) \approx \Phi_{h0}^{1/2}(\omega_1^2 + \omega_2^2)^{-\beta/2} \tag{15}$$

where $\Phi_{h0}^{1/2}$ is an arbitrary constant and β is the required spectral exponent of the output fBm approximant $y(n_1, n_2)$. The frequency domain (ω_1, ω_2) is *continuous* on R^2 and $M(\omega_1, \omega_2)$ is rectangularly-periodic at integer multiples of 2π along ω_1 and ω_2. Consequently, we shall approximate $M(\boldsymbol{\omega})$ in (12) over the region of $\boldsymbol{\omega}$ given by

$$R_\pi^2 \equiv \{\omega_1, \omega_2 \in R^2| - \pi \leq \omega_{1,2} \leq \pi\} \tag{16}$$

where unit spatial sample distances are assumed; that is, $n_{1,2} \in Z$.

Although there is a significant body of literature relating to 2D circularly-symmetric frequency responses [7], the design of 2D filters according to (12) is non-trivial. Given the 2D discrete transform transfer function $H(z_1, z_2) \equiv Z[h(n_1, n_2)]$ in the matrix form

$$H(z_1, z_2) = \frac{[1 z_1^{-1} z_1^{-2} \cdots z_1^{-K_1}][\mathbf{A}]}{[1 z_1^{-1} z_1^{-2} \cdots z_1^{-K_1}][\mathbf{B}]} \times \frac{[1 z_2^{-1} z_2^{-2} \cdots z_2^{-K_2}]^T}{[1 z_2^{-1} z_2^{-2} \cdots z_2^{-K_2}]^T} \tag{17}$$

we require a stable implementation having acceptably low orders K_1 and K_2 and a magnitude response $M(\omega_1, \omega_2) = |H(e^{j\omega_1}, e^{j\omega_2})|$ that approximates $M(\boldsymbol{\omega})$ of (12) in R_π^2.

Domain of the Approximation It is most important that $M(\omega_1, \omega_2)$ be approximated in a satisfactory way in the region R_π^2. *Near the origin* of R_π^2, say where $||\boldsymbol{\omega}||_2 < \pi/10$, *it is particularly important that the approximation be valid* because this region of the ω domain corresponds to the surface features that are readily detectable by the human vision system as landscape features. If the image $y(n_1, n_2)$ has support $Z^2 \equiv \{n_1, n_2| - M_i/2 \leq n_i \leq M_i/2, \forall n_i, i = 1, 2\}$, then there is no reason to maintain the fBm approximation at frequencies closer to the origin than about $||\omega||_2 < \pi/M_i$ because the corresponding spatial-domain features have spatial-constants that exceed the size $M_1 \times M_2$ of the image and cannot be viewed. The accuracy of the fBm approximation is also non-critical in regions well-removed from the origin, where $||\boldsymbol{\omega}||_2 > \pi/4$, because such spectral components do not contribute significantly to overall perceived shape but, rather, to the fine texture of the perceived surface.

A. Approximation of fBm Using a 2D Recursive Digital Filter Employing Rotated 1D Filters

Consider the radial line L_i in R_π^2, at an angle θ_i as shown in Fig. 2. We shall design a rotated 1D recursive digital filter $H_i(z_1, z_2)$ having a 2D magnitude frequency response given

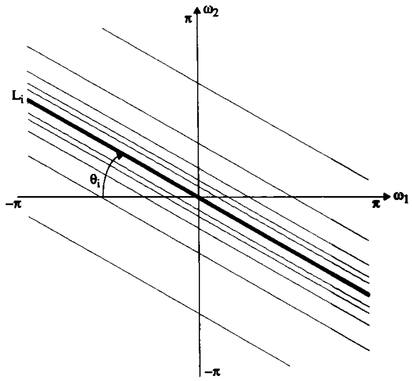

Fig. 2. Radial line about which $M_i(\gamma_i)$ is defined.

by some appropriate function $M_i(\gamma_i)$ where

$$\gamma_i = \omega_1 \cos\theta_i + \omega_2 \sin\theta_i \tag{18}$$

In directions parallel to L_i, the gain $M_i(\gamma_i)$ is therefore constant, as indicated by the gain contours shown in Fig. 2.

Consider now the set of N radial lines L_i shown in Fig. 3, corresponding to equi-spaced radial lines in R_π^2 given by

$$\theta_i = -\frac{\pi}{2} + \frac{\pi i}{2N}, \quad i = 0, 1, \ldots, N-1 \tag{19}$$

and the corresponding rotated-1D filters $H_i(z_1, z_2)$ having the gain functions $M_i(\gamma_i)$. The serial connection of such N rotated-1D filters has the transform transfer function

$$H(z_1, z_2) = \prod_{i=1}^{N} H_i(z_1, z_2) \tag{20}$$

and frequency response

$$M(\omega_1, \omega_2) = \prod_{i=1}^{N} M_i(\gamma_i) \tag{21}$$

Clearly, $M(\omega_1, \omega_2)$ has $2N$-side polygonal symmetry about the origin and *not* the circular symmetry that we are seeking. Further, we have so far not determined how to select the function M_i. It is shown in Appendix A that, with

$$M_i(\gamma_i) \equiv \frac{1}{(\gamma_i)^\lambda}, \tag{22}$$

substituting (22) into (21) gives the 2D magnitude frequency response

$$\begin{aligned} M(\omega_1, \omega_2) &= \prod_{\substack{k=0 \\ k\neq i}}^{N-1} \frac{1}{(\|\boldsymbol{\omega}\|_2 \sin\delta_k)\lambda} \\ &= \left[\prod_{\substack{k=0 \\ k\neq i}}^{N-1} (\sin\delta_k)^{-\gamma}\right] \prod_{\substack{k=0 \\ k\neq i}}^{N-1} \frac{1}{[\|\boldsymbol{\omega}\|_2]^\lambda} \end{aligned}$$

2D FREQUENCY RESPONSE OF N ROTATED 1D FILTERS ALONG L_i (23)

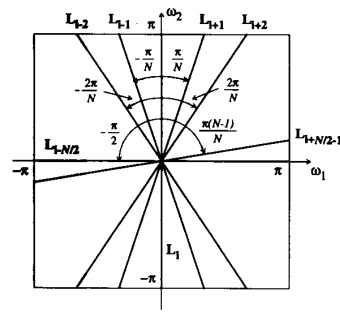

Fig. 3. N rotated functions $|H_i(e^{j\omega_1}, e^{j\omega_2})|$.

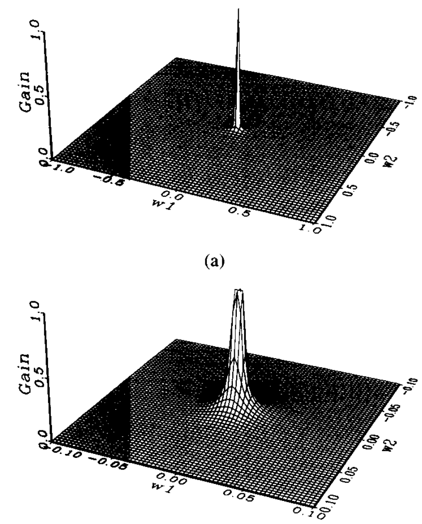

(a)

(b)

Fig. 4. Ideal $M(\omega_1, \omega_2)$ from (14) with $\beta = 3$ shown on frequency axes normalized to π, (a) $-\pi \leq \omega_1, \omega_2 \leq \pi$. (b) $-.1\pi \leq \omega_1, \omega_2 \leq .1\pi$.

where the angle δ_k is shown in Fig. 3 and is given, for any line L_i, $i = 0, 1, 2, \ldots, N$, by

$$\delta_k = -\frac{\pi}{2} + \frac{\pi k}{N}, \; k = 0, 1, \ldots, N-1 \tag{24}$$

The magnitude response in (23) exactly matches the required circularly-symmetric magnitude response along all N radial lines L_i if we choose the spectral exponent λ as

$$\lambda = \frac{\beta}{2(N-1)} \quad \text{SPECTRAL EXPONENT OF 1D FILTER PRIOR TO ROTATION} \tag{26}$$

B. 2D Numerical Example, $N = 6$, $\beta = 3$

We want to simulate 2D fBm in an image $y(n_1, n_2)$ having size $(M_1, M_2) = (512, 512)$ and having a fractal dimension $D = 2$; that is, according to (2) and (4), $\beta = 3$. Then, from (12), the required magnitude frequency response of the 2D filter, when driven by 2D white noise, has the form $M(\omega_1, \omega_2) = \Phi_0^{1/2}(\omega_1^2 + \omega_2^2)^{-3/2}$, which is shown on a linear vertical axis in Figs. 4(a) and 4(b). The most important region of R_π^2, $-\pi/10 < \omega_1, \omega_2 < \pi/10$, is shown in Fig. 4(b).

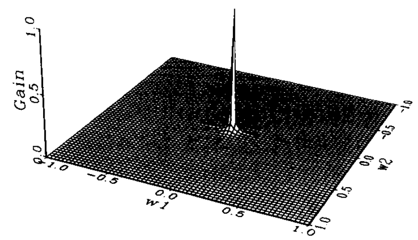

(a)

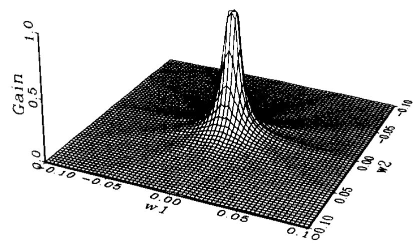

(b)

Fig. 5. $M(\omega_1, \omega_2)$ approximated via (21) shown on frequency axes normalized to π, (a) $-\pi \le \omega_1.\omega_2 \le \pi$, (b) $-.1\pi \le \omega_1.\omega_2 \le .1\pi$.

Consider the choice $N = 6$, corresponding to the six lines $L_1, L_2, \ldots, L_6$ in angular increments of $\pi/6$, according to (19). From (26), we choose $\lambda = 0.3$ and use (18)–(22) to obtain the approximation of $M(\omega_1, \omega_2)$ shown in Figs. 5(a) and 5(b) which closely approximates the required $M(\omega_1, \omega_2) = \Phi_0^{1/2}(\omega_1^2 + \omega_2^2)^{-3/2}$ shown in Figs. 4(a) and 4(b). It is concluded that we may use these six rotated 1D filters to implement the required 2D filter.

V. 2D Filter Implementation Using Six Rotated 1D Filters and a Sub-Sampling Scheme

Consider the six lines $L_1, L_2, \ldots, L_6$ shown in Fig. 6. The six 1D filters $H_i(z_1, z_2)$ used in (20) are to be designed from a continuous-domain lowpass prototype function

$$P(s) = \frac{[c_0 c_1 \cdots c_K][1 s \cdots s^K]^T}{[d_0 d_1 \cdots d_K][1 s \cdots s^K]^T} \tag{27}$$

The discrete-domain prototype filter $G(z)$ may then be obtained by the bilinear transformation as

$$\begin{aligned} G(z) &\equiv P(s)\big|_{s=\frac{2}{T}\frac{z-1}{z+1}} \\ &= \frac{[a_0 a_1 \cdots a_K][1 z^{-1} \cdots z^{-K}]^T}{[b_0 b_1 \cdots b_K][1 z^{-1} \cdots z^{-K}]^T} \end{aligned} \tag{28}$$

where T is the intersample distance on the rectangular sample grid and where $P(s)$ is designed such that

$$M(\omega) \equiv |G(e^{j\omega})| = M_0|\omega|^{-\lambda}, \tag{29}$$

as required.

The two *axis-aligned* filters, corresponding to L_1 and L_4, can be implemented simply as $H_1(z_1, z_2) = G(z_1)$ and $H_4(z_1, z_2) = G(z_2)$, respectively. Now consider $H_2(z_1, z_2)$, corresponding to alignment on the off-axis line L_2 in Fig. 6.

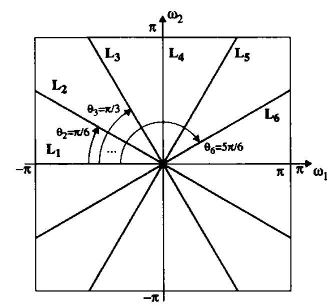

Fig. 6. Six rotated 1D filters.

The rotated function $H_2(z_1, z_2)$ can be obtained from (27) by the conventional s-domain rotation

$$s = s_1 \cos\theta_1 + s_2 \sin\theta_1 \tag{30}$$

such that

$$H_2(z_1, z_2) = P(s_1 \cos\theta_2 + s_2 \sin\theta_2)\big|_{s_{1,2}=\frac{2}{T_{1,2}}\frac{z_{1,2}-1}{z_{1,2}+1}} \tag{31}$$

Similarly, the 3 other off-axis filters, corresponding to L_i, $i = 3, 5, 6$, can be obtained as

$$H_i(z_1, z_2) = P(s_1 \cos\theta_i + s_2 \sin\theta_i)\big|_{s_{1,2}=\frac{2}{T_{1,2}}\frac{z_{1,2}-1}{z_{1,2}+1}} \tag{32}$$

However, we have chosen *not* to employ this conventional approach to the design of the s-domain-rotated 2D filters along $L_i, i = 2, 3, 5, 6$, but instead to use a *sub-sampling technique* that corresponds to *1D filters along lines* $L'_i, i = 2, 3, 5, 6$. These lines are very close to the lines $L_i, i = 2, 3, 5, 6$. The implementation of 1D filters provides improved computational efficiency relative to the corresponding 2D filters obtained in (31) and (32). We note that, for L_2, $\tan(\theta_2) = \tan(\pi/6) = 0.577$. We choose the line L'_2 having angle θ'_2 such that $\tan(\theta'_2) = 0.50$. Similarly, we choose L'_i and $\theta'_i, i = 3, 5, 6$, as follows:

$$\begin{aligned} \tan(\theta'_3) &= 2.0 \\ \tan(\theta'_5) &= -2.0 \\ \tan(\theta'_6) &= -0.5. \end{aligned} \tag{33}$$

The lines L'_2, L'_6 exactly intersect the *sub-sample points* $(2n_1, n_2)$, as shown in Fig. 7, and the lines L'_3, L'_5 exactly intersect the sub-sample points $(n_1, 2n_2)$. We propose to design 1D filters $G_i(z), i = 2, 3, 5, 6$, that *have their sample points along the lines* $L'_i, i = 2, 3, 5, 6$, implying that their frequency responses on ω_1, ω_2 are rotated versions of the 1D filter response $M(\omega) = M_0|\omega|^{-\lambda}$. The 1D filters are easily designed from $G(z)$; we need only take into account the increased intersample distance of $T = \sqrt{5}$ in (28). Let $G_{\sqrt{5}}(z)$ denote the discrete-domain prototype function that corresponds to (28) with $T = \sqrt{5}$. For the line L'_2, we employ the 1D filter $H_2(z_1, z_2) = G_{\sqrt{5}}(z_1, z_2) \equiv G_2(z)$, where the shift operator $z = z_1^2 z_2$ and corresponds to a shift by two pixels in n_1 and one pixel in n_2, *which is implemented as a* 1D *recursion*

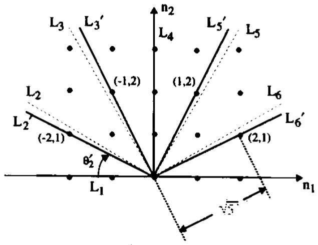

Fig. 7. Lines L_2', L_3', L_5', L_6', suitable for 1D filter implementation.

TABLE I
COEFFICIENTS OF 1D PROTOTYPE FUNCTION HAVING $\lambda = 0.3$ AND $M = 3$

	k	0	1	2	3
$P(s)$	c_k	-0.0034291	-0.056713	-0.051339	0.19965
	d_k	0.0037880	0.16226	0.78074	1.0
$G(z)$	a_k	0.08817	-0.61461	0.69672	-0.19771
	b_k	1.9468	-3.6071	2.06837	-0.37773
$G_{\sqrt{5}}(z)$	a_k	-0.021202	-0.078959	0.078921	-0.006193
	b_k	0.32196	-0.34058	0.050994	-0.0020715

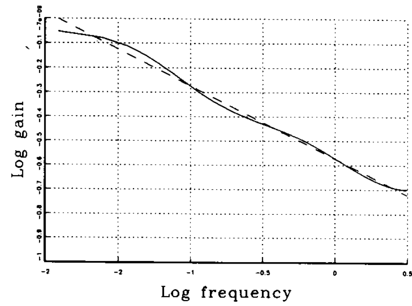

Fig. 8. Numerically optimized $M(\omega)$ of the 1D prototype function (solid line) and ideal response (dashed line), $K = 3$ and $\lambda = 0.3$.

along the line L_2'. Similarly, the remaining sub-sampled 1D filters are given by

$$\begin{aligned} H_3(z_1, z_2) &= G_{\sqrt{5}}(z_1 z_2^2) \equiv G_3(z) \\ H_5(z_1, z_2^2) &= G_{\sqrt{5}}(z_1^{-1} z_2^2) \equiv G_5(z) \\ H_6(z_1, z_2) &= G_{\sqrt{5}}(z_1^{-2} z_2) \equiv G_6(z). \end{aligned} \tag{34}$$

The final 2D transfer function of the required filter is then given by

$$\begin{aligned} H(z_1, z_2) = \prod_{i=1}^{6} G_i(z) &= G(z_1) \cdot G(z_2) \cdot G_{\sqrt{5}}(z_1^2 z_2) \cdot \\ & G_{\sqrt{5}}(z_1 z_2^2) \cdot G_{\sqrt{5}}(z_1^{-1} z_2^2) \cdot G_{\sqrt{5}}(z_1^{-2} z_2) \end{aligned}$$

FRACTAL GENERATING FILTER (35)

A. Design of the s-Domain Prototype Filter $P(s)$

The coefficients of a third-order ($K = 3$) prototype function $P(s)$ corresponding to (27) and (29) and with $\lambda = 0.3$ have been obtained by the conventional numerical optimization of $M(\omega)$ to approximate that in (29) and are given in Table I along with the coefficients for both $G(z)$ and $G_{\sqrt{5}}(z)$. The numerically-optimized magnitude frequency response $M(\omega) = |G(e^{j\omega})|$ is shown in Fig. 8 along with the ideal response $M_0|\omega|^{-\lambda}$. Note that the zero-frequency gain $M(0)$ is tapered to unity, for practical reasons. The 2D frequency response $M(\omega_1, \omega_2) = |H(e^{j\omega_1}, e^{j\omega_2})|$, from (35), is shown in Figs. 9(a) and 9(b). This 2D frequency response closely approximates the required function $M(\omega_1, \omega_2) = \Phi_0^{1/2}(\omega_1^2 + \omega_2^2)^{-3/2}$ and therefore the filters in Table I are used to simulate 2D fractal landscapes. The contours of $M(\omega_1, \omega_2)$ are approximately circular and the function rolls off along the lines L_i in close agreement with $\Phi_0^{1/2}(\omega_1^2 + \omega_2^2)^{-3/2}$, as shown in Fig. 10 for the case of L_1, L_4. Between these lines, the contours in Fig. 9 confirm that the approximation remains good within the required domain of approximation in R_π^2.

Given the order K for $G(z)$, the total number of calculations for each complete 1D recursion is $(2K+1)M_1 M_2$ real multiplications and real additions. The total number of calculations for all N 1D filtering operations is therefore

$$\begin{aligned} N_{\text{add}}^{(\text{IIR})} &= N(2K+1)M_1 M_2 \\ N_{\text{mult}}^{(\text{IIR})} &= N(2K+1)M_1 M_2. \end{aligned} \tag{36}$$

A comparison of (36) with the DFT method and (9) confirms that the proposed method is computationally more efficient for very large images (typically where $M_1, M_2 \gg 8192$). For an image of dimension $M_1 = M_2 = 16,384$, and using $N = 6$ and $K = 3$ for the prototype filter, a total of 11.274×10^9 real multiplications and additions are required. This compares to 15.032×10^9 real multiplications and 22.549×10^9 real additions for the 2D FFT method by (9). For smaller images, say $M_1 = M_2 = 512$, the relative computational advantage is less significant. For example, 11,010,048 real multiplications and additions are required for the proposed method and 9,437,184 real multiplications and 14,155,776 real additions are required for the DFT method.

B. Example: A 2D Simulated Fractal Landscape Image with Spatially-Variant Roughness

The proposed method may be used to simulate a fractal landscape of dimension $M_1 = M_2 = 128$ having surface features that are determined by the *spatially-variant* spectral exponent $\beta(n_1, n_2)$, as shown in Fig. 11, from which we expect relatively smooth landscape "terrain" in the lower-left region, $\beta(n_1, n_2) = 4.0$, that becomes progressively more rugged where $\beta(n_1, n_2)$ tends to the lower limit of 3.0. A transition zone is used to change $\beta(n_1, n_2)$ gradually and consists of 9 rings, each 4 pixels in width, as shown. $\beta(n_1, n_2)$ is decreased in increments of 0.1 through the 9 rings, from 4.0 at the interior boundary of the zone to 3.0 at the exterior boundary. Corresponding 1D prototype functions $P(s), G(z), G_{\sqrt{5}}(z)$, having $\lambda = 0.4, 0.39, 0.38, \ldots, 0.31$,

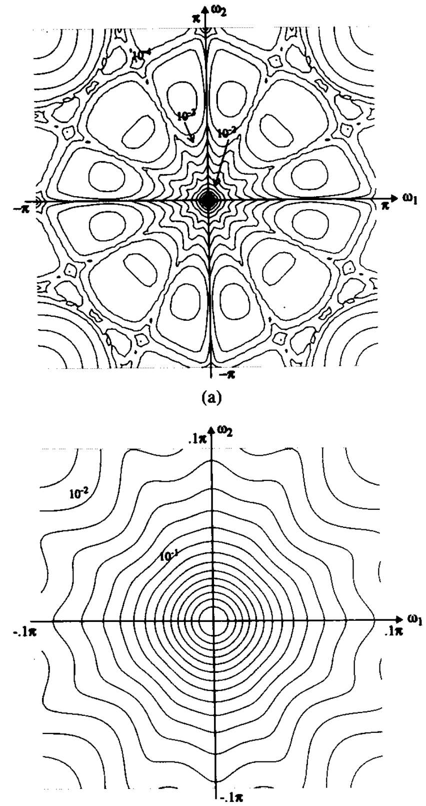

Fig. 9. Contour diagrams of $M(\omega_1, \omega_2)$ using (33), (a) $-\pi \leq \omega_1 . \omega_2 \leq \pi$, (b) $-.1\pi \leq \omega_1 . \omega_2 \leq .1\pi$.

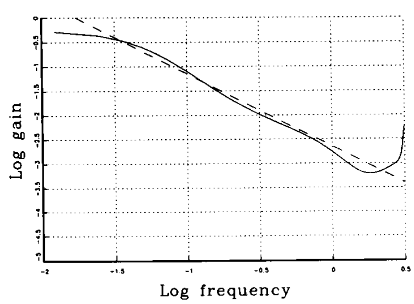

Fig. 10. Cross-section of $M(\omega_1, \omega_2)$ in Fig. 9(a) along lines L_1 and L_4.

have been designed by numerical optimization and their s-domain coefficients are provided in Table II.

The 1D recursion is performed on each of the lines $L_1, L_2', L_3', L_4, L_5', L_6'$, as described above. The spatial variation of $\beta(n_1, n_2)$ is achieved *during the recursion on each line* by simply switching to the coefficients of the appropriate $G(z)$ or $G_{\sqrt{5}}(z)$ at each pixel where $\beta(n_1, n_2)$ changes value. Employing a 128 × 128 white noise source (implying $\alpha = 0$) as the input signal to the spatially-variant set of six rotated 1D filters gives the 128 × 128 fractal landscape image $y(n_1, n_2)$ shown in Fig. 12. The fractal dimension D of the surface

TABLE II
COEFFICIENTS OF TEN 1D PROTOTYPE FUNCTIONS HAVING $\lambda = 0.40$ TO 0.31

k		0	1	2	3
$\lambda = 0.40$	c_k	-0.0023016	-0.034643	-0.042271	0.111625
	d_k	0.0025777	0.13165	0.70491	1.0
$\lambda = 0.39$	c_k	-0.0024078	-0.036518	-0.043158	0.12272
	d_k	0.0026954	0.13505	0.71380	1.0
$\lambda = 0.38$	c_k	-0.0024976	-0.03826	-0.044267	0.12955
	d_k	0.0027938	0.13751	0.72006	1.0
$\lambda = 0.37$	c_k	-0.002601	-0.040198	-0.045253	0.13676
	d_k	0.002906	0.14046	0.72759	1.0
$\lambda = 0.36$	c_k	-0.002709	-0.04226	-0.046152	0.14437
	d_k	0.0030235	0.14357	0.73542	1.0
$\lambda = 0.35$	c_k	-0.0028183	-0.044377	-0.047151	0.15238
	d_k	0.0031417	0.14654	0.74281	1.0
$\lambda = 0.34$	c_k	-0.0029303	-0.04660	-0.048061	0.16085
	d_k	0.0032622	0.14955	0.75024	1.0
$\lambda = 0.33$	c_k	-0.0030525	-0.049001	-0.048863	0.16979
	d_k	0.0033919	0.15285	0.75830	1.0
$\lambda = 0.32$	c_k	-0.0031759	-0.051461	-0.049768	0.17921
	d_k	0.0035231	0.15599	0.76587	1.0
$\lambda = 0.31$	c_k	-0.0033066	-0.054095	-0.050545	0.18915
	d_k	0.0036609	0.15935	0.77389	1.0

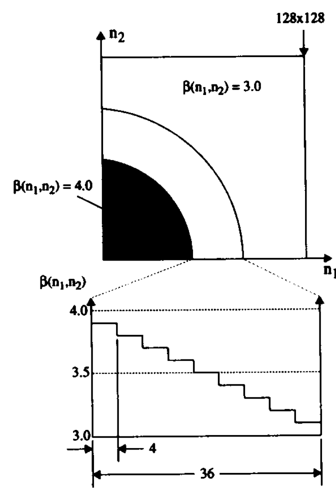

Fig. 11. Profile of spectral exponent used in spatially-varying 2D recursive filter example.

increases from the front-left corner to the far-right corner, implying progressively increasing "roughness" as the recursion proceeds away from the front-left corner.

VI. SUMMARY

In this contribution, we show that MD recursive digital filtering techniques may be employed to simulate MD random fBm. Hyperspherically-symmetric MD recursive filters may be used to filter MD input noise images that have known

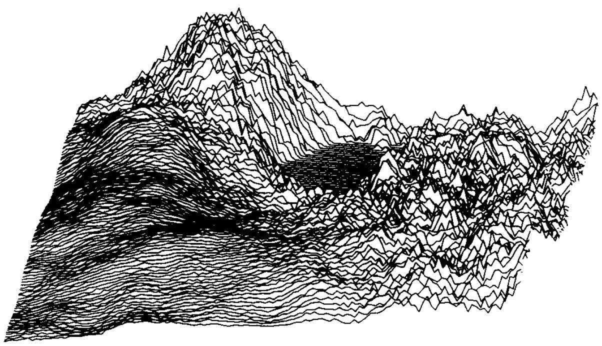

Fig. 12. Simulated fractal landscape produced by spatially-varying 2D recursive filtering.

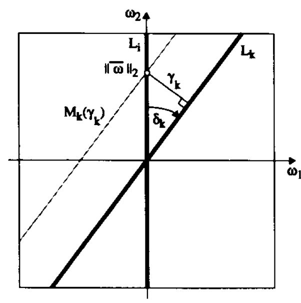

Fig. A1. Intersection of the contours of $M_k(\gamma_k)$ with L_i.

MD spectral density functions, producing realistic MD random fractal images directly in the spatial domain. The method improves upon current DFT-based methods of simulating MD fBm by eliminating the undesirable edge effects produced by the DFT and by permitting local variation of the surface characteristics by spatially varying the spectral exponent β according to the location of the recursion in the image. This technique has been demonstrated in this contribution for 2D fractal landscape images. A 2D recursive filter has been used to approximate the required circularly-symmetric magnitude frequency response using six rotated 1D recursive filters.

Appendix A

In this appendix, we derive (23), which is the 2D frequency response along each line L_i of the serial connection of N rotated 1D filters. Consider two lines, L_i and $L_k, k \neq i$, where L_k is rotated from L_i by an angle δ_k, as shown in Fig. A1. From (22), $M_k(\gamma_k) = 1/(\gamma_k)^\lambda$ where $\gamma_k = \omega_1 \cos\delta_k + \omega_2 \sin\delta_k$. Hence, $M_k(\gamma_k)$ has gain contours that are parallel to the line $\gamma_k = \omega_1 \cos\delta_k + \omega_2 \sin\delta_k = 0$. We wish to determine the contribution of $M(\gamma_k)$ to the overall 2D magnitude frequency response $M(\omega_1, \omega_2)$ along L_i. Consider a point $\|\omega\|_2 = (\omega_1^2 + \omega_2^2)^{1/2}$ on L_i, as shown in Fig. A1. The contour of $M_k(\gamma_k)$ that intersects L_i at $\|\omega\|_2$ corresponds to $\gamma_k = \|\omega\|_2 \sin\delta_k$, as shown in Fig. A1. Therefore, the 2D magnitude frequency response $M(\omega_1, \omega_2)$ along L_i due to $M_k(\gamma_k)$ is

$$M(\omega_1, \omega_2) = M_k(\|\omega\|_2 \sin\delta_k) = \frac{1}{(\|\omega\|_2 \sin\delta_k)^\lambda} \tag{A1}$$

All $M_k(\gamma_k), k \neq i$, contribute in this way to $M(\omega_1, \omega_2)$ along L_i, giving (23) for δ_k given in (24).

References

[1] B. B. Mandelbrot, "Forward: People and Events Behind the 'Science of Fractal Images'," *The Science of Fractal Images*, Heinz-Otto Peitgen and Dietmar Saupe, Eds., New York: Springer-Verlag, 1988, pp. 1–19.

[2] R. J. Voss, "Fractals in Nature: from Characterization to Simulation," *The Science of Fractal Images*, Heinz-Otto Peitgen and Dietmar Saupe, Eds., New York: Springer-Verlag, 1988, pp. 21–70.

[3] P. Flandrin, "Wavelet analysis and synthesis of fractional brownian motion," *IEEE Trans. on Info. Theory*, vol. 38, no. 2, pp. 910–917, Mar. 1992.

[4] A. H. Tewfik and M. Kim, "Correlation structure of the discrete wavelet coefficients of fractional brownian motion," *IEEE Trans. on Info. Theory*, vol. 38, no. 2, pp. 904–909, Mar. 1992.

[5] M. S. Keshner, "1/f Noise," *Proc. IEEE*, vol. 70, no. 3, Mar. 1982, pp. 212–218.

[6] D. Saupe, "Algorithms for random fractals," *The Science of Fractal Images*, Heinz-Otto Peitgen and Dietmar Saupe, Eds., New York: Springer-Verlag, 1988, pp. 71–136.

[7] P. K. Rajan and M. N. S Swamy, "Design of separable denominator 2-dimensional digital filters possessing real circularly symmetric frequency responses," *Proc. IEE*, Pt. G, vol. 129, no. 5, Oct. 1982, pp. 235–240.

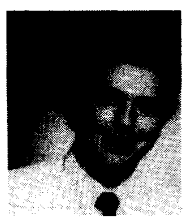

Norman R. Bartley (S'75–M'78) received the B.Sc. and M.Sc. degrees in electrical engineering from the University of Calgary, Calgary, Alberta, Canada, in 1976 and 1978, respectively.

He is currently employed at the University of Calgary as a Research Associate. His main fields of interest include multidimensional systems, image processing, and digital signal processing systems and architectures.

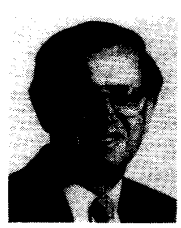

Leonard T. Bruton (SM'80–F'81) is a Professor of Electrical Engineering at the University of Calgary, Calgary, Alberta, Canada. His research interests are in the area of analog and digital signal processing. He is particularly interested in the design and implementation of microelectronic digital filters and the applications of multidimensional circuit and systems theory to digital image processing.